Title

Size-Resolved Chemical Composition of Sub-20 nm Particles from Methanesulfonic Acid Reactions with Methylamine and Ammonia

Journal

ACS Earth and Space Chemistry, 4(7)

ISSN

2472-3452

Authors

Perraud, Véronique
Li, Xiaoxiao
Jiang, Jingkun
et al.

Publication Date

2020-07-16

DOI

10.1021/acsearthspacechem.0c00120

ACS EARTH AND SPACE CHEMISTRY

http://pubs.acs.org/journal/aesccq

Article

Size-Resolved Chemical Composition of Sub-20 nm Particles from Methanesulfonic Acid Reactions with Methylamine and Ammonia

Véronique Perraud,[§] Xiaoxiao Li,[§] Jingkun Jiang, Barbara J. Finlayson-Pitts,* and James N. Smith*

Cite This: *ACS Earth Space Chem.* 2020, 4, 1182−1194

Read Online

ACCESS | Metrics & More | Article Recommendations | Supporting Information

ABSTRACT: Particle formation in the atmosphere from gas-phase precursors has been observed around the world; however, our fundamental understanding of the key species responsible and mechanisms involved remains uncertain. Recent laboratory studies demonstrated that acid−base reactions involving methanesulfonic acid (CH_3SO_3H, MSA) and small alkylamines may contribute significantly to new particle formation. To date, most of the investigations have been focused on particle number concentration and size distribution measurements in combination with quantum chemistry predictions of the most stable clusters. Here, we present the first measurements of the size-resolved chemical composition of sub-20 nm particles generated in a custom flow reactor from the reaction of MSA with methylamine (MA) in the presence or absence of NH_3 using thermal desorption chemical ionization mass spectrometry (TDCIMS). A novel design of the TDCIMS inlet was evaluated, and the measurement of the chemical composition of particles was extended down to 5 nm in diameter, the smallest size yet reported for this method. MSA−MA particles with diameters smaller than 9 nm were found to be more acidic, with an acid/base molar ratio of 1.8 ± 0.4 (1σ) for 5 nm particles compared to the larger particles which were neutral. A similar acid/base molar ratio trend was observed when NH_3 was added to the MSA−MA combination. In the MSA−MA−NH_3 system, the MA/NH_3 molar ratio was higher than 1 (up to 2.6) for all particle sizes despite the much larger concentration of NH_3 in the gas phase (the gas-phase MA/NH_3 ratio was ∼0.23), indicating that MA is a key component in particle formation from this system. The potential reasons for this based on previous calculations of small clusters in this system are discussed.

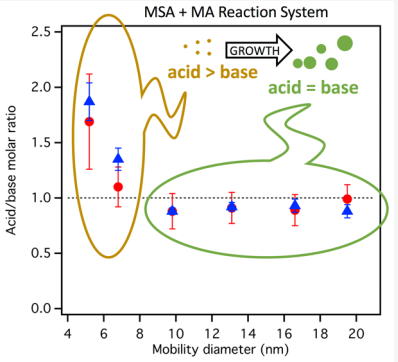

KEYWORDS: *methanesulfonic acid, methylamine, ammonia, thermal desorption chemical ionization mass spectrometry, new particle formation, nanoparticles*

1. INTRODUCTION

New particle formation (NPF) is an important and ubiquitous secondary transformation process in the atmosphere,[1−3] contributing to a majority of the global aerosol population and about half of the global low-level cloud condensation nuclei (CCN) population.[4−7] The first step in NPF is the formation of stable clusters from gaseous vapors.[8−14] The newly formed stable clusters, which are typically smaller than ∼2 nm, can only act as CCN after taking up condensable vapors and growing to sizes above 50−100 nm.[15−17] This growth process, which can last for hours or days in the atmosphere depending on the growth rates,[1] is also important for scattering light efficiently[18−20] and for deep penetration into the lungs.[21−23] Competing with condensational growth is coagulation with pre-existing particles,[24,25] which is significant for sub-20 nm particles. Thus, understanding all of these processes is crucial for addressing the uncertainty associated with not only aerosol−cloud−climate interactions but also particle effects on visibility and health.

Acid−base reactions have been proven to play a significant role in laboratory and field studies of nucleation and growth processes.[1−3,26−34] While most studies to date have focused on H_2SO_4−ammonia/amine nucleation systems,[2,28−30,34] recent investigations have demonstrated that methanesulfonic acid (CH_3SO_3H; MSA) can also efficiently initiate NPF in the presence of small alkylamines and water.[31−33,35−38] In air, MSA is one of the oxidation products of organosulfur compounds such as dimethyl sulfide, which is widely emitted from biological ocean processes, agriculture, industry, and domestic activities.[39−45] The ambient concentration of gas-phase MSA (∼10^5 to 10^7 molecules cm^{-3}) can be of the same order of magnitude as that of H_2SO_4.[46−49] In addition, the newly formed particles measured in a boreal forest[50] and in the Finnish Arctic[51] were observed to be enriched in MSA. Particulate MSA was also observed to correlate with NPF occurring in the summertime in the Arctic.[52−54] Furthermore, with the current decreasing trend of anthropogenic SO_2

Received: May 4, 2020
Revised: June 23, 2020
Accepted: June 24, 2020
Published: June 24, 2020

https://dx.doi.org/10.1021/acsearthspacechem.0c00120
ACS Earth Space Chem. 2020, 4, 1182−1194

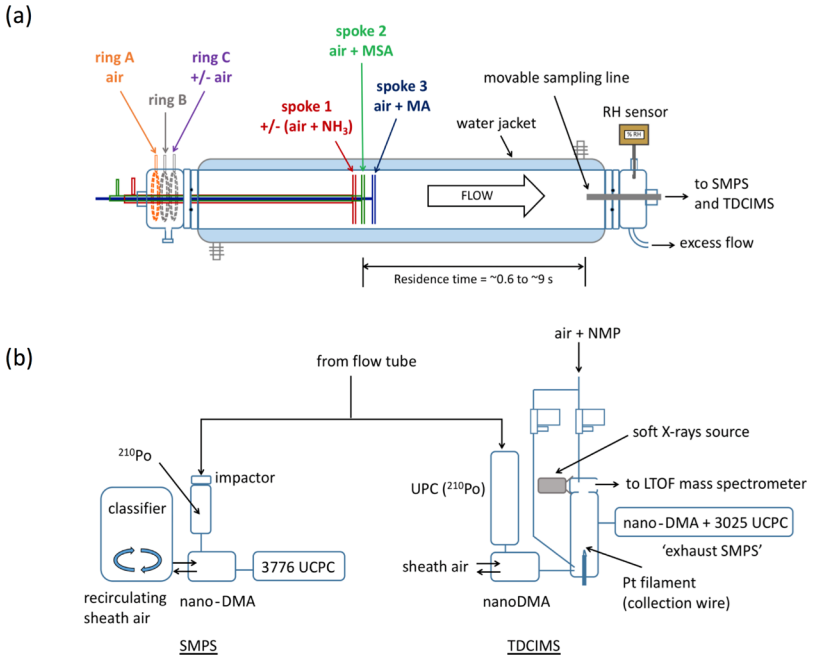

Figure 1. (a) Schematic of the 1 m borosilicate flow reactor (adapted from ref 35). Flows were distributed as follows: ring A, 4.2 L min^{-1}(air only); spoke 2, 2.0 L min^{-1} (mixture of MSA diluted in air); and spoke 3, 1.2 L min^{-1} (mixture of MA diluted in air). For the MSA + MA system, an additional air flow (1.0 L min^{-1}) was added through ring C, while for the MSA + MA + NH_3 system, the air flow was moved down to spoke 1 and mixed with the flow of NH_3 (total flow at spoke 1, 2.0 L min^{-1}). (b) Simplified diagram of the sampling train including the SMPS and thermal desorption chemical ionization mass spectrometer apparatus. NMP = *N*-methylpyrrolidone; nano-DMA = nanodifferential mobility analyzer; UCPC = ultrafine condensation particle counter; and UPC = unipolar charger.

emissions[55−60] and the increasing rate at which polar sea ice is melting, which gives rise to increasing phytoplankton productivity and as a consequence higher dimethyl sulfide and MSA concentrations,[61−64] NPF initiated from MSA acid−base chemistry may become more important in the future.[55]

Ammonia and amines are important atmospheric bases and originate from a variety of sources, including animal husbandry, biomass burning, urban settings, sewage and solid waste treatment, forest floor, and marine environments.[65−75] Although the concentrations of amines are typically much smaller than that of ammonia, amines have been shown both theoretically and experimentally to be much more efficient than NH_3 in NPF with both H_2SO_4 and MSA.[31,32,34,76−80] Amines were also found to replace NH_3 in H_2SO_4−NH_3 and MSA−NH_3 clusters and particles.[81−84] Further, remarkable synergies in the form of enhancement of NPF have been recently observed for both H_2SO_4 and MSA-related multicomponent systems where NH_3 was present simultaneously with an amine.[77,78,85−88] For example, Perraud et al.[87] demonstrated that the presence of NH_3 enhanced NPF from the acid/base-initiated chemistry between MSA and trimethylamine (TMA) up to 6 orders of magnitude. As a result, this system was extremely efficient at nucleating and growing particles to detectable sizes, while the corresponding MSA + TMA binary system was not efficient on its own. Additionally, only a modest effect was observed for the MSA + MA system, which is already extremely efficient. Last, amines and ammonia are often found along with MSA in particles around the world.[50,89−93] For instance, Lawler et al.[50] detected both MSA and alkylamines in 20−70 nm nanoparticles in the Hyytiälä boreal forest during a nucleation event.

An improved understanding of NPF from acid−base chemistry requires direct measurements of the size-resolved chemical composition of particles formed, especially over the diameter range from ∼2 to 20 nm. Such measurements are challenging because of the small mass loadings, low signal-to-noise ratio, and the need to remove the interferences from both larger particles and gas-phase species. To date, two approaches have shown success at measuring size-resolved, sub-10 nm diameter particle composition. The nano aerosol mass spectrometer,[94,95] equipped with a digital ion trap reflection time-of-flight mass detector, allows the elemental composition of individual nanoparticles to be measured down to 7 nm. Thermal desorption chemical ionization mass spectrometry (TDCIMS)[96−100] has been shown to determine the size-resolved composition of particles with diameters down to 6 nm with molecular information and a limit of detection of several picograms.

Recently, size-resolved nanoparticles formed from laboratory-controlled H_2SO_4 reactions with NH_3 and dimethylamine[101,102] and HNO_3 + dimethylamine systems[103] have been studied using TDCIMS to gain insights into chemical composition through their acid/base ratios. Results from the Cosmics Leaving Outdoor Droplets (CLOUD) study indicated that 10−15 nm particles from H_2SO_4 + dimethylamine + NH_3 were acidic but became neutral after growing above 15 nm.[101,104] A similar trend was observed in laboratory flow reactor experiments examining H_2SO_4 + dimethylamine and H_2SO_4 + NH_3 systems where particles smaller than 12 nm were not fully neutralized in the presence of excess gas-phase base.[102] Chee et al.[103] conducted nucleation and growth studies by reacting a monoprotic acid, nitric acid (HNO_3), with dimethylamine and found that the particles were nearly neutral above 9 nm (smaller particles were unable to be measured for this system).

https://dx.doi.org/10.1021/acsearthspacechem.0c00120
ACS Earth Space Chem. 2020, 4, 1182−1194

Here, we have extended these measurements to another acid−base system of atmospheric relevance, the reaction of MSA with MA, in the presence or absence of NH_3. TDCIMS equipped with a new high-resolution time-of-flight mass spectrometer (LTOF mass analyzer, Tofwerk AG) was used to detect the size-resolved chemical composition of sub-20 nm particles, extending the diameter range down to 5 nm. A new feature of the instrument is the application of soft X-rays as the ionization source and the use of a new ionization reagent for the detection of NH_3 and amines. This new implementation was essential to the success of the present study, and some analytical aspects are described. From the TDCIMS measurements, the size-resolved acid/base molar ratios were determined, and possible growth mechanisms are discussed.

2. EXPERIMENTAL METHODS

2.1. Flow Reactor Description. A 1 m borosilicate glass flow reactor, described in detail elsewhere,[35,36,87] was used to produce nanoparticles from the reaction of MSA with MA in the presence or absence of NH_3. The flow reactor was operated with two configurations illustrated in Figure 1 and described below. The sequence of addition of reactants was as follows: 4.2 L min^{-1} of dry clean air was injected in the first ring (ring A); 0.2 L min^{-1} of gas-phase MSA mixed with 1.8 L min^{-1} of dry clean air was added through the second spoke (spoke 2); and 0.2 L min^{-1} of gas-phase MA mixed with ∼1.0 L min^{-1} of dry clean air was added through the third spoke (spoke 3) through holes that face upstream. In MSA + MA only experiments (i.e., in the absence of NH_3), an additional 1.0 L min^{-1} of dry clean air was introduced through ring C. In experiments with NH_3, the 1.0 L min^{-1} of air flow was moved from ring C down to spoke 1 and increased to 1.5 L min^{-1}, to which 0.5 L min^{-1} of gas-phase NH_3 was added. The stream of the NH_3/air mixture was introduced radially so that when MSA (spoke 2) was introduced into the flow reactor, it would react with both MA and NH_3 at the same time. The total flow rates under these conditions were 8.4 L min^{-1} (MSA + MA only) and 9.4 L min^{-1}(in the presence of NH_3). A purge air generator (Parker−Balston; model 75-62) provided the dry clean air used in all experiments. Further details of dry clean air purification can be found in the Supporting Information. All experiments were carried out at 1 atm and 298 K and under dry conditions with the relative humidity maintained at <3% as indicated by a humidity probe (Vaisala; model HMT 838). All flows were controlled by high-precision mass flow controllers (Alicat or MKS) and were periodically confirmed with a flow calibrator (Sensidyne; Gilibrator 2). The flow reactor was cleaned regularly with nanopure water (18.2 MΩ cm; Thermo Scientific, Barnstead; model 7146) and dried with dry clean air with the water jacket set at 343 K. The flow reactor was conditioned with a flow of gas-phase MSA for at least 2 days after cleaning prior to an experiment.

Particle size distributions and chemical composition measurements were performed, as described below, using a movable stainless steel sampling line (o.d. 0.635 cm) located inside the flow reactor along the centerline of the reactor and placed at distances ranging from 3 to 43 cm away from spoke 2 (i.e., the MSA addition port). Based on a conversion factor determined in previous studies,[35] these distances correspond to residence times ranging from 0.64 to 9.1 s for the MSA + MA system and 0.59 to 8.5 s for the MSA + MA + NH_3 system. For simplicity, the shorter residence time is hereafter referred as ∼0.6 s and the longest residence time as ∼9 s for both systems. Note that the residence time reported here does not account for the time spent in the sampling line (∼1.1 s) as NPF and growth are expected to cease because of the losses on the walls of the sampling line.

2.2. Reactants. Gas-phase MSA was generated by passing 0.2 L min^{-1} of dry purge air over the pure liquid (Sigma-Aldrich, ≥ 99%) contained in a glass trap maintained at room temperature and introduced into the flow tube through spoke 2. Commercially available permeation tubes (VICI Metronics) containing pure NH_3 or MA were used to generate the gas-phase bases. Each permeation tube was enclosed inside a U-shaped glass tube. The flow of air over the MA permeation tube was 0.2 L min^{-1}, while that of NH_3 was 0.5 L min^{-1}. To ensure a constant temperature, the MSA glass trap and the amine permeation tubes were immersed in a water bath maintained at room temperature (T = 293 K). The concentration of each species introduced into the flow reactor was measured routinely (details of the measurements can be found in the Supporting Information). The initial concentrations after dilution in the flow reactor for MSA, MA, and NH_3 (when present) were (2.1−2.3) × 10^{11} molecules cm^{-3} (8.4−9.3 ppb), (1.3−1.4) × 10^{11} molecules cm^{-3} (5.3−5.8 ppb), and 5.8 × 10^{11} molecules cm^{-3} (23.5 ppb), respectively. These concentrations represent upper limits as they do not account for wall losses. Note that higher concentrations than ambient of reactants were required in these studies in order to fulfill the limits of detection of TDCIMS, allowing the characterization of the chemical composition of these particles with reasonable collection times.

2.3. Particle Size Distribution Measurements. Particle size distributions were continuously measured using a scanning mobility particle sizer (SMPS) consisting of a 0.071 cm impactor nozzle, a ^{210}Po radioactive source (NRD LLC; model P-2021), a TSI model 3080 electrostatic classifier equipped with a nanodifferential mobility analyzer (nano-DMA; TSI, Inc.; model 3085), and a butanol-based ultrafine condensation particle counter (UCPC; TSI, Inc.; model 3776). The sheath air flow was set to 15 L min^{-1} (recirculating mode), and the aerosol flow was 1.5 L min^{-1}, which provided measurements of the size distributions over the mobility diameter range of 2−64 nm.

2.4. Size-Resolved Online Chemical Composition Measurements. The size-resolved chemical composition for the 5−20 nm diameter nanoparticles was measured by TDCIMS.[100−102] Briefly, the sample (3 L min^{-1}) was passed first through a unipolar charger (UPC)[100,105] to generate negatively charged particles that were subsequently size-selected using a nano-DMA running in low resolution mode[106] with a sheath flow of 10 L min^{-1} (sheath-to-aerosol flow ratio ∼3.3). Instead of recirculating the sheath gas in the nano-DMA, dry clean air was used as the sheath flow to prevent the accumulation of gas-phase MSA, MA, or NH_3. The particles were then directed to an electrostatic precipitator where a high voltage (+3 kV) was applied to a Pt filament to collect the particles. During collection, the filament was flushed with dry clean air to prevent the capture of gas-phase species. After collection for 1−720 min, depending on the aerosol mass concentration, the filament was translated into the ion source, where it was resistively heated using a temperature ramp up to ∼600 °C to desorb the particle components. Note that the wall of the desorption area was maintained at 50 °C during the measurement to reduce condensation of the evaporated material to the walls. The desorbed species were then ionized

https://dx.doi.org/10.1021/acsearthspacechem.0c00120
ACS Earth Space Chem. 2020, 4, 1182−1194

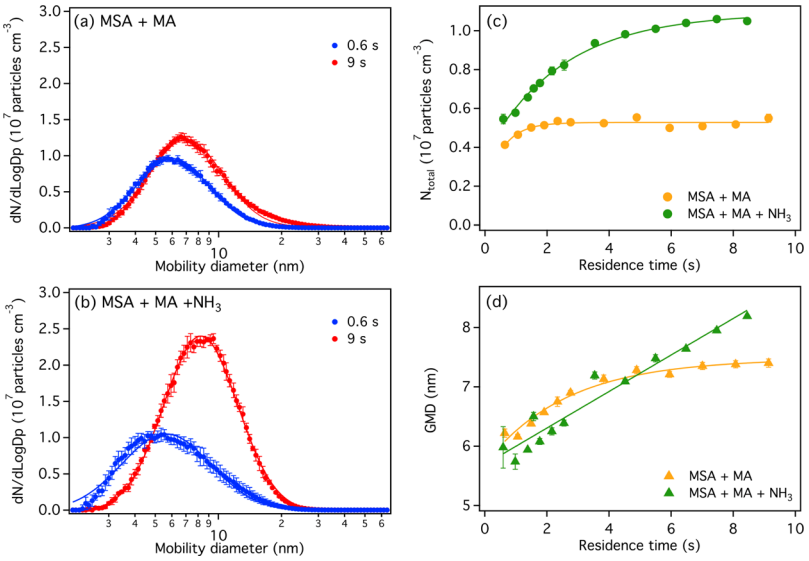

Figure 2. Size distributions for (a) MSA + MA and (b) MSA + MA + NH_3 reaction systems collected at ∼0.6 and ∼9 s residence times. Each size distribution is the average over 5−15 individual scans with the error bars representing 1 standard deviation. The lines are log-normal fits to guide the eye. (c) Corresponding total particle number concentrations (N_{total}) and (d) GMDs measured as a function of residence time. The lines are fits to guide the eye. For all panels, the initial concentrations of reactants are [MSA] = (2.1−2.3) × 10^{11} molecules cm^{-3} (8.4−9.3 ppb); [MA] = (1.3−1.4) × 10^{11} molecules cm^{-3} (5.3−5.8 ppb); and [NH_3] = 0 or 5.8 × 10^{11} molecules cm^{-3} (23.5 ppb).

via chemical ionization using a soft X-ray source (Hamamatsu Photonics Ltd; photoionizer model L9490, emitting at 3−9.5 keV). The resulting ions were analyzed by an LTOF.

TDCIMS can be performed in both positive and negative ion modes: MSA was measured in the negative ion mode with $(H_2O)_nO_2^-$ (n = 0−2) as the reagent ion, while both NH_3 and MA were measured in the positive ion mode with either $(H_2O)_nH_3O^+$ (n = 0−2) alone or added N-methylpyrrolidone (NMP; C_5H_9NO; MW = 99 g mol^{-1}). We previously showed[107] that NMP exhibits good sensitivity and selectivity for measuring NH_3 and amines via the formation of $[M + NMP + H]^+$ and $[M + 2NMP + H]^+$ ions (where M represents either MA or NH_3); this is its first application as an ionization reagent in TDCIMS. Note that the soft X-ray source illuminated the entire ionization volume of the ion source. Although chemical ionization should be the main ionization pathway, the possibility that some of the ions detected by the LTOF are produced by direct ionization by the soft X-rays cannot be ruled out. No evidence for additional chemistry was observed.

An entire TDCIMS measurement cycle included four steps: (1) cleaning mode: the filament was set to the home position and was resistively heated up to 600 °C for 1 min to clean any residues on the filament; (2) cooling mode: the filament was cooled down to room temperature for ∼30 s; (3) collection mode: as described above (1−720 min); and (4) analysis mode: the filament was moved from the collection position into the ionization source where it was resistively heated by the application of a power-controlled ac current for a total duration of 70 s. Each collection cycle was followed by a background cycle where no collection voltage was applied to the Pt filament. Background-subtracted spectra, where the spectra from the background cycle (i.e., when no particles are collected on the filament) are subtracted from the sample spectra (i.e., when size-selected particles have been collected on the filament and subsequently thermally desorbed and analyzed by the mass spectrometer), were used for quantification. Last, an "exhaust SMPS" consisting of a nano-DMA and a UCPC (model 3025, TSI, Inc.) was used to detect the particles downstream of the electrostatic precipitator. The particle mass collected on the filament was estimated from these exhaust SMPS measurements by differencing the particle size distributions obtained during the collection and background cycles.

New aspects of the instrument included the switch from nitrogen to dry clean air as the carrier gas throughout the instrument and the use of a soft X-ray source in place of the ^{210}Po radioactive source to generate the reagent ions (O_2^-, H_3O^+, and $[NMP + H]^+$). Thus, some fragmentation and ionization patterns with this new design may be different from the previous TDCIMS experiments and were remeasured in this study.

The size distributions of the particles generated in the flow tube were stable over days (Figure S1). This made it possible to explore the size-resolved chemical composition over long collection time periods. The shortest (∼0.6 s) and longest (∼9.0 s) residence times from both experiments were selected in order to produce the largest span of particle sizes, the latter being an indicator of nanoparticle age. The chemical composition of 5.2, 6.8, 9.8, 13.1, 16.6, and 19.5 nm particles was measured for each condition. The collected mass on the filament from all of the experiments in this study was between 0.16 and 4.5 ng, with collection times ranging from 1 to 720 min. For particles smaller than 5.2 nm, the sample mass was too small to be detected with 720 min collection time. For particles larger than 19.5 nm, the uncertainties increase significantly because of low particle number concentration, low filament collection efficiency, and multiply charged particles produced by the UPC.

2.5. Atomized Reference Particles. In order to determine the accurate TDCIMS acid/base signal ratio between MSA and MA and NH_3, reference MSA−MA and MSA−NH_3 particles were generated using a constant output atomizer (TSI, Inc.; model 3076). Aqueous solutions comprising 0.5 mM equimolar concentrations of MSA and

https://dx.doi.org/10.1021/acsearthspacechem.0c00120
ACS Earth Space Chem. 2020, 4, 1182−1194

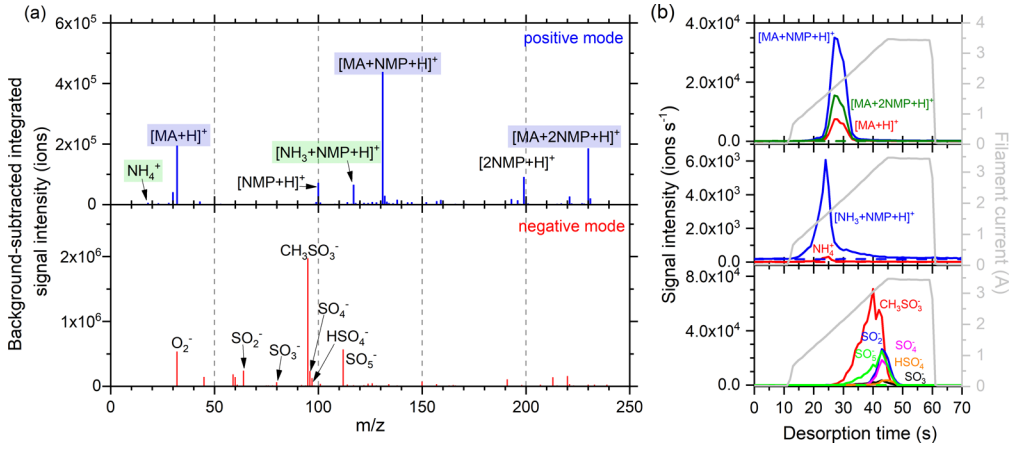

Figure 3. (a) Representative background-subtracted integrated mass spectra in the positive ion mode (top blue trace) and negative ion mode (bottom red trace) summed over the desorption period for analysis of MSA−MA−NH_3 particles collected from the flow reactor. In those, the spectra from the "background" cycle (i.e., when no particles are collected on the filament) were subtracted from the "sample" spectra (i.e., when size-selected particles have been collected on the filament and subsequently thermally desorbed and analyzed by the mass spectrometer). As a result, the reagent ions are subtracted out, which yields background-subtracted spectra where the ions corresponding to the component of the particles (MA or MSA) are clearly visible. The corresponding raw spectra (before background subtraction) are displayed in Figure S4. (b) Corresponding desorption profiles of the ions related to MA, NH_3 and MSA during the "analysis mode" and the filament desorption current profile (gray trace), which is directly related to the filament temperature.

MA or MSA and NH_3 were atomized using dry purge air (36 psi) as the carrier gas. For these, liquid standards of MSA (Sigma-Aldrich; ≥ 99%), MA (Sigma-Aldrich; 40% w/w in water), and NH_3 (Aldrich; 28.7% w/w in water) were used. The flow exiting the atomizer was 2 L min^{-1} and was passed through two diffusion driers (TSI, Inc.; model 3062-NC) containing silica gel beads (Delta Adsorbents; 4 × 8 mesh). The flow of dry particles was then diluted with an additional 3 L min^{-1} of dry, clean air before being sampled by the SMPS operated in the low flow mode (i.e., aerosol flow rate, 0.3 L min^{-1}; sheath flow rate, 3.0 L min^{-1}) as well as by the TDCIMS. Polydisperse atomized MSA−MA particles were additionally measured using a sequential spot sampler,[108,109] followed by ion chromatography (Dionex) and liquid chromatography mass spectrometry [ultra-performance liquid chromatography−electrospray ionization−tandem mass spectrometry (UPLC−ESI−MS/MS), Waters, Quattro Premier XE]. The details of these measurements can be found in the Supporting Information.

3. RESULTS AND DISCUSSION

3.1. Nanoparticle Size Distributions in the Presence or Absence of NH_3. Figure 2 displays the size distributions for MSA + MA (Figure 2a) and MSA + MA + NH_3 (Figure 2b) particles generated in the flow tube at ∼0.6 and ∼9 s residence times, respectively. Under these conditions, a large number of sub-20 nm particles formed quickly, as indicated by the size distributions observed at ∼0.6 s in both systems, with a total number concentration (N_{total}) of (4.1 ± 0.03) × 10^6 and (5.5 ± 0.2) × 10^6 particles cm^{-3}, respectively. The particle geometric mean diameter (GMD) in both experiments was ∼6 nm at 0.6 s residence time (Figure 2d). Note that previous laboratory studies have demonstrated that MSA + MA is an efficient acid/base system for nucleating particles,[31,32,35,87,110] and the intent of this particular investigation was primarily the generation of a range of particle sizes in order to collect enough mass within a reasonable sampling time for size-resolved TDCIMS measurements. Evolution of the size distribution as a function of residence time in the flow tube is presented in the Supporting Information (Figure S2 a,b). In the MSA + MA system, N_{total} increased slightly from ∼0.6 to 2 s (Figure 2c) and then remained constant, indicating that either the limiting reactant is consumed quickly and/or the reaction is complete. The distribution of particles collected at 9 s had a GMD of 7.4 nm (Figure 2d).

Upon the addition of NH_3 (5.8 × 10^{11} molecules cm^{-3}), NPF was systematically enhanced compared to the MSA + MA system at all residence times, with N_{total} about double that observed in the absence of NH_3 at ∼9 s residence time. This enhancement is consistent with that observed in a previous study.[87] Evolution of N_{total} as a function of time (Figure 2c) shows that NPF was occurring continuously up to ∼8 s residence time in the presence of NH_3. As can be seen in Figure 2d, at early residence times, the GMD was typically smaller for the MSA + MA + NH_3 system compared to the binary MSA + MA system which, combined with the increase in N_{tot}, suggests that NH_3 promotes NPF. However, at longer residence times, in the presence of NH_3, the GMD was slightly larger with a GMD of 8.2 nm at ∼9 s residence time. At earlier stages of growth, the concentration of gaseous precursors/clusters is high enough to support the formation of new particles as well as the growth of newly formed particles. At later stages of growth, gaseous precursors/clusters are depleted, slowing down both nucleation and growth of particles. Note that the MSA + NH_3 nucleation system was much less efficient on its own in forming particles, with N_{total} of only 3.2 × 10^5 particles cm^{-3} (Figure S3) measured at ∼9 s compared to 5.5 × 10^6 particles cm^{-3} for the binary MSA + MA system (Figure 2c) and 1.05 × 10^7 particles cm^{-3} for the MSA + MA + NH_3 system (Figure 2c). These results are consistent with the previous reports of synergy initiated by NH_3 in binary H_2SO_4 + amine[77,78] and binary MSA + amine systems.[87]

3.2. Size-Resolved Chemical Composition Measurements by TDCIMS. *3.2.1. Ion Distributions Measured by TDCIMS and Their Thermal Desorption Profiles.* Methylamine (MA) was detected in the positive ion mode as three different ions (Figure 3a, top blue trace), including [MA + H]+

https://dx.doi.org/10.1021/acsearthspacechem.0c00120
ACS Earth Space Chem. 2020, 4, 1182−1194

(m/z 32), $[MA + NMP + H]^+$ (m/z 131), and $[MA+2NMP + H]^+$ (m/z 230), produced from the reaction of MA with $(H_2O)_nH_3O^+$, $[NMP + H]^+$, and $[2NMP + H]^+$, respectively. The $[MA + NMP + H]^+$ adduct was the most abundant signal in the background-subtracted integrated spectra, about 2−3 times more intense than the $[MA + H]^+$ ion. For NH_3, the dominant signal was also the $[NH_3 + NMP + H]^+$ adduct at m/z 117, with a signal about 15 times greater than that of the NH_4^+ ion. No other ions were observed in the positive ion mode (a typical raw positive ion mass spectrum is shown in Figure S4a).

In the negative ion mode (Figure 3a, bottom red trace; Figure S4b), the dominant ion in the background-subtracted integrated spectra observed for MSA was the deprotonated parent $CH_3SO_3^-$ ion at m/z 95, followed by five additional minor ions, which included SO_2^- (m/z 64), SO_3^- (m/z 80), SO_4^- (m/z 96), HSO_4^- (m/z 97), and SO_5^- (m/z 112). These ions were attributed to fragments of MSA consistent with the recently reported mass spectra of pure MSA and sodium methanesulfonate salt using soft ionization in direct analysis in real time MS.[111] A linear relationship was observed between SO_2^- and SO_4^- signal intensities as well as between SO_3^- and SO_5^-, suggesting that these ions have a common origin. It was previously proposed[101,102] that SO_5^- was formed from the reaction of O_2^- with SO_3 in the analysis of H_2SO_4. However, because of the difference in their respective electron affinities (EAs), O_2^- ions are expected to react with SO_2/SO_3 by charge transfer to form SO_2^-/SO_3^- ions [EAs for SO_2 (1.107 eV) and SO_3 (1.97 eV) being higher than that of O_2 (0.451 eV)].[112] In earlier studies,[113,114] it was proposed that SO_2^- ions can immediately associate back with O_2 to form SO_4^- ions. By analogy to these studies, we propose that both ions observed here, SO_4^- and SO_5^-, correspond to $[SO_2+O_2]^-$ and $[SO_3+O_2]^-$ adducts, respectively. The minor HSO_4^- ion was attributed to the potential OH chemistry occurring in the ion source.[111] The distribution of the different ions was similar across all the flow reactor experiments.

Figure 3b shows the current applied to the filament (gray line) and the thermal desorption profiles for ions related to MA, NH_3 and MSA during the 70 s analysis period in a typical MSA + MA + NH_3 experiment. For the first 10 s, no current was applied to the filament while it remained at room temperature. During the next 35 s, the current increased linearly from 0 to 3.4 amps, and the temperature increased to an estimated ∼600 °C. The temperature remained at its highest level for another 15 s. Finally, the current was removed from the filament, and the temperature quickly fell back to room temperature. Each signal intensity was close to zero before heating the filament, indicating that there is no evaporation for any of the species collected on the filament at room temperature. When the temperature rose, NH_3 was the first species to evaporate from the particles, followed by MA, and finally MSA. This is in accordance with the saturation vapor pressures (P_{sat}) of each component: $P_{sat}(NH_3)$ = 9.8 atm;[115] $P_{sat}(MA)$ = 3.5 atm;[112] and $P_{sat}(MSA) = 7.4 \times 10^{-7}$ atm.[116] The signal returned to zero at the end of the desorption period, indicating that no residue was left on the filament after a heating cycle. The quick and thorough desorption of the species is an advantage for quantification. The subsequent background measurements (no current applied to the filament) were very clean, indicating that the contribution from the gas phase was negligible and there was no significant residue on the filament.

As described in detail in the Supporting Information (Figure S5), the background-subtracted integrated signal observed for MA, NH_3, and MSA from MSA−MA−NH_3 particles collected (D_p = 19.5 nm) at the end of the flow reactor was linear for a collection time up to 10 min for MA and MSA and for a longer time period for NH_3 (40 min). For higher mass loading, depletion of the reagent ions occurred. When the reagent ions were not depleted, the good linearity across the species indicated that the collection time did not significantly influence their detection and that the evaporation of MA, NH_3, and MSA from the sampled particles was negligible during the collection period, which allowed quantitative measurements of the particle acid/base molar ratios.

3.2.2. Size-Resolved Acid/Base Molar Ratios. The relative sensitivity of TDCIMS for MSA, MA, and NH_3 was first investigated using atomized MSA−MA and MSA−NH_3 particles generated from equimolar MSA + MA and MSA + NH_3 solutions. Surprisingly, ammonium ions were systematically detected by TDCIMS in particles formed by atomizing an equimolar solution of MSA + MA. Independent measurements using the sequential spot sampler also exhibited high amounts of NH_4^+ for those particles (Figure S6a). From measurements by both the thermal desorption chemical ionization mass spectrometer and the spot sampler, MA/NH_3 molar ratios were estimated to range from ∼2 to 4. Two studies previously reported the presence of ammonium from atomized aqueous solutions of dimethylamine and H_2SO_4.[101,117] In these cases, it was suspected that it was due to the presence of trace amounts of NH_3 in either the nanopore water[77] used to prepare the solution or the gas supply. Another possibility is that the trace amount of NH_3 from room air permeated through the Teflon tubing containing the atomized particles. Lawler and co-workers[101] excluded the formation of NH_4^+ inside TDCIMS by analyzing the aqueous H_2SO_4-dimethylamine solution itself, which exhibited no ammonium ions. Similarly, in the present studies, the aqueous solution used in the atomizer did not contain any detectable ammonium by IC (Supporting Information Figure S6b), although ammonium was systematically measured in particles formed by atomizing the same solution. The resulting MSA/MA molar ratio for those particles was estimated from the IC and UPLC−MS measurements to be 1.5, and the acid/base signal ratio (or sensitivity factor) recorded by TDCIMS for the MSA + MA atomized particles ($F_{MSA/MA}$) was corrected for that (see the Supporting Information for details). The final relative sensitivities (Figure S7) were 6.6 ± 1.1 for MSA/MA ($F_{MSA/MA}$) and 99 ± 15 for MSA/NH_3 (F_{MSA/NH_3}). These two sensitivities were then used to convert the measured acid/base signal ratios for particles formed in the flow tube from MSA + MA and MSA + MA + NH_3 reactions systems into acid/base molar ratios as details in the Supporting Information.

Figure 4 shows the size-resolved acid/base molar ratios in the MSA + MA nucleation from gas-phase precursors measured at the shortest (∼0.6 s) and longest (∼9 s) residence times. At ∼0.6 s, the acid/base molar ratio for particles with diameters (D_p) of 5.2 and 6.8 nm was 1.9 ± 0.2 (1σ) and 1.4 ± 0.1 (1 σ), respectively, while for larger particles (D_p > 9 nm), it was close to unity. This indicates that the particles were acidic at 5.2 and 6.8 nm (i.e., contained more acid molecules than base) but became neutral as they grew to 9.8 nm. A similar trend was found for particles collected at ∼9

https://dx.doi.org/10.1021/acsearthspacechem.0c00120
ACS Earth Space Chem. 2020, 4, 1182−1194

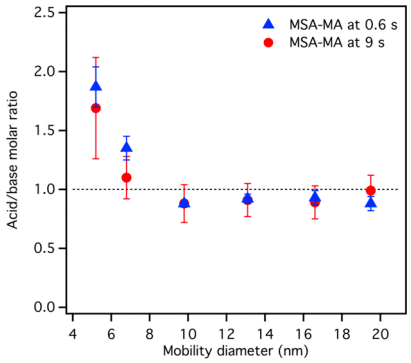

Figure 4. Size-resolved acid/base ratios determined for the particles in the MSA + MA system at ~0.6 s (blue) and ~9 s (red) residence times. The error bars represent 1 standard deviation from at least three repeated measurements. The horizontal dashed line represents an acid/base molar ratio of 1, corresponding to neutral particles. The initial concentrations of reactants are [MSA] = 2.3×10^{11} molecules cm^{-3} (9.3 ppb) and [MA] = 1.4×10^{11} molecules cm^{-3} (5.8 ppb).

s residence time, indicating a similar growth mechanism over the diameter range.

Figure 5a shows the size-resolved acid/base molar ratios for the MSA + MA + NH_3 system. At ~0.6 s residence time, the trend with particle size is similar to that for the MSA + MA system, with smaller particles (D_p < 7 nm) being more acidic

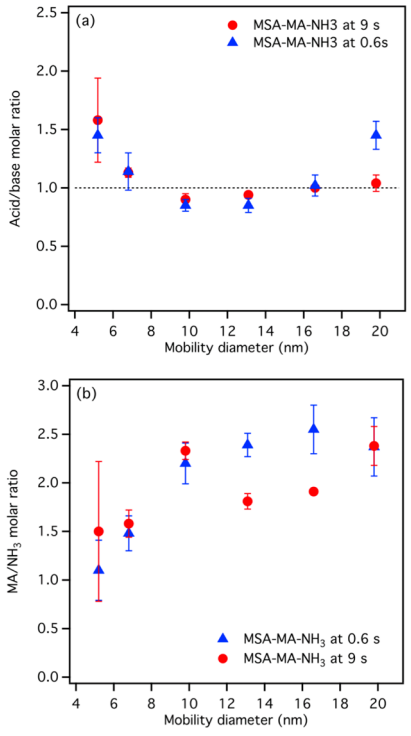

Figure 5. (a) Size-resolved acid/base ratios determined for the particles in the MSA + MA + NH_3 nucleation system at ~0.6 s (blue) and ~9 s (red) residence times. Here, "base" refers to the sum of NH_3 and MA mole concentrations. The error bars represent 1 standard deviation from at least three repeated measurements. The horizontal dashed line represents an acid/base ratio of 1; (b) MA/NH_3 molar ratios as a function of particle mobility diameter. The initial concentrations of reactants are [MSA] = 2.1×10^{11} molecules cm^{-3} (8.4 ppb); [MA] = 1.3×10^{11} molecules cm^{-3} (5.3 ppb); and [NH_3] = 5.8×10^{11} molecules cm^{-3} (23.5 ppb).

and larger particles exhibiting a molar acid/base ratio close to unity. Note that the particles at 19.5 nm appear to be more acidic at 0.6 s but not at 9 s. As shown in Figure 5b, the MA/NH_3 molar ratio measured at 0.6 s was 1.1 ± 0.3 (1σ) for 5.2 nm particles and increased with diameter to reach ~2.5 for particles larger than 10 nm. The particles measured at the longer residence time (9 s) exhibited a similar increasing trend with diameter. Note that the particle phase MA/NH_3 ratio (~2) is much larger than the gas-phase ratio between the two bases (~0.23), indicating that MA is the key component in NPF, although NH_3 has a synergistic effect as reported recently.[87]

3.2.3. Discussion. A summary of the enthalpies of formation of each cluster determined in previous quantum chemical calculations[31,118] for a series of MSA−MA clusters is given in Figure 6. In this figure, only selected growth paths are

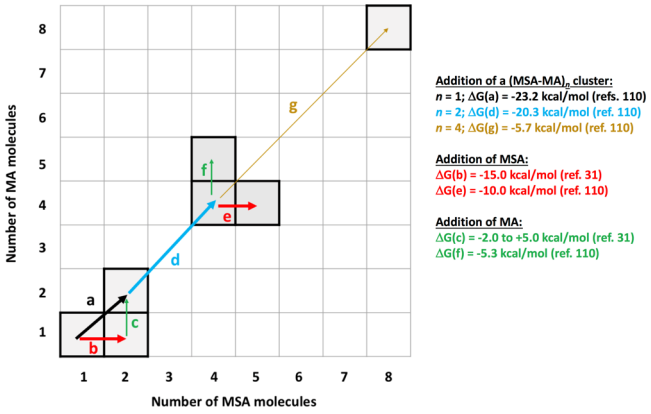

Figure 6. Matrix representing potential growth pathways for selected MSA−MA clusters following the Gibbs free energy (ΔG) of the addition of MSA, MA, or a $(MSA-MA)_n$ cluster (n = 1, 2, or 4) based on previous quantum simulations (from refs 31 and 110). Note that the matrix only represents the mechanistic paths reported in those two studies. The thickness of the arrow represents the preference for the growth of the cluster, where a thick arrow represents a favorable route for the cluster to grow.

represented based on those previous studies, where thick arrows correspond to the most favorable paths by which a cluster can grow (i.e., paths a, b, d, and e), and thin arrows (path c, f, and g) correspond to less favorable routes. Calculations of dissociation energies, enthalpies, and free energies have indicated that $(MSA-MA)_4$ is a major intermediate in the growth process.[110,118] This cluster, which approaches 1 nm in size, was found to be thermodynamically stable with calculated dissociation-free energies (ΔG) of 66.8 kcal mol^{-1} for the $(MSA-MA)_4 \rightarrow 4$ (MSA−MA) reaction and 20.3 kcal mol^{-1} for the $(MSA-MA)_4 \rightarrow 2$ $(MSA-MA)_2$ reaction. The lifetime of the $(MSA-MA)_4$ cluster is greater than 100 picosecond (ps) at T = 300 K.[118] The same study indicated that the growth of the cluster via addition of MSA to $(MSA-MA)_4$ is favorable, with a Gibbs free energy of −10 kcal mol^{-1} for the addition reaction,[118] while that for MA addition was less favorable, with a Gibbs free energy of −5.3 kcal mol^{-1} for the addition reaction. Thermodynamic simulations performed at T = 300 K indicated that MSA does not evaporate from the MSA−$(MSA-MA)_4$ cluster in 100 ps, while MA can dissociate from MA−$(MSA-MA)_4$ cluster in just 3.5 ps.[118] The incorporation of a second MSA molecule to the initial (MSA−MA) ion pair, forming a MSA−(MSA−MA)

https://dx.doi.org/10.1021/acsearthspacechem.0c00120
ACS Earth Space Chem. 2020, 4, 1182−1194

cluster, was also previously predicted to be favorable (ΔH = −29 kcal/mol and ΔG = −15 kcal/mol).[31]

The mechanism for MA to be taken up into particles is via acid/base interactions[119] with an MSA molecule either present in the gas phase as a free species forming an ion pair, or neutralizing a cluster enriched in MSA. However, ΔG for the addition of MA to the MSA−(MSA−MA) cluster, resulting in full neutralization, is relatively high, between −2 and +5 kcal/mol depending on the point of addition and the cluster structure (path c in Figure 6).[31] This one-on-one growth mechanism (favorable addition of the acid, followed by a higher energetic barrier for the addition of a base, i.e., growth of the (MSA−MA) cluster following path b and then path c) was previously demonstrated to occur in the H_2SO_4 + NH_3 system. In the latter case, similar to the MSA−MA clusters, a lower energy barrier was observed for the addition of an acid molecule to an existing cluster (close to collision limited uptake), followed by a much higher barrier for the addition of the base to yield neutralization.[120,121] All these calculations are consistent with the prevalence of small acidic clusters.

The growth of the $(MSA−MA)_4$ unit cluster from collision with another cluster (path g in Figure 6) was found to be somewhat favorable (ΔG = −5.7 kcal/mol), where the $(MSA−MA)_4$−$(MSA−MA)_4$ cluster is thermodynamically stable for at least 100 ps at T = 300 K.[118] More recent simulations on MSA−MA clusters using the Atmospheric Cluster Dynamics Code[122] support the findings from these earlier studies, where neutral clusters and clusters with higher numbers of MSA than MA were observed to be the most stable. Together, these calculations are qualitatively consistent with the observed higher acidity of the smallest particles in the MSA−MA system and the neutral state of the larger particles. These observations parallel experiments that examined H_2SO_4 acid−base reactions, where the growth mechanism was shown to be not only driven by H_2SO_4 addition (i.e., monomer−cluster collision) but also driven by cluster−cluster collisions when high concentrations of gas-phase bases are present.[26,27,123]

The influence of NH_3 on various MSA−base binary systems,[87] including MSA + MA, was recently investigated using quantum simulations, which show that the $(NH_3)_2$−$(MSA−MA)_2$ cluster does not show any significant changes in its general structure compared to the $(MSA−MA)_2$ cluster. In both, the proton transfer is from the MSA to MA; however, NH_3 is shown to stabilize the cluster, consistent with the enhancement of the particle number concentration observed in the current study (Figure 2c). In this case, the preference of the proton for MA follows the gas-phase basicity, which is higher for MA (864.5 kJ mol^{-1}) compared to that of NH_3 (819 kJ mol^{-1}).[124] Thermodynamic modeling studies indicated that the (MSA−MA) cluster exhibits a proton transfer between the acid and the base, forming a stable ion pair that could interact with an existing cluster as described above. This, however, is not the case for the $(MSA−NH_3)$ cluster, which is only stabilized by van der Waals forces that are much weaker.[118,125] Olenius et al.[126] demonstrated that H_2SO_4−NH_3 clusters grow via stepwise addition of the acid, followed by the base, whereas H_2SO_4−dimethylamine clusters, where dimethylamine binds more strongly to the acid, grow via collision with other acid−base clusters. This is consistent with MA being much more effective than NH_3 in nucleation and growth of new particles in our experiments. This is also consistent with the observation of high MA/NH_3 molar ratios (∼2) in the particles, despite the concentration of gas-phase NH_3 being ∼4 times higher than that of MA in the experiments.

4. CONCLUSIONS

Reactions of MSA with MA efficiently lead to the formation of sub-20 nm particles. The size-resolved chemical composition of the nanoparticles measured with TDCIMS shows that the smallest particles (D_p < 9 nm) are more acidic, while the acid/base molar ratio approaches unity (neutral) as particles grow to larger sizes. This trend in acidity is consistent with the addition of MSA molecules to the neutral clusters being favorable thermodynamically.[31,118] On the other hand, condensation of MA or NH_3 is comparatively less favorable, and these species are expected to partition back to the gas phase. Salt formation (either forming acid−base ion pair clusters in the gas phase or via neutralization by reactive uptake of the amine onto an acidic particle) can explain the larger neutral particles. The trend for MSA−amine systems is similar to previous observations reported for H_2SO_4 + dimethylamine, H_2SO_4 + dimethylamine + NH_3, and H_2SO_4 + NH_3 systems.[101,102,104]

Finally, the addition of NH_3 to the MSA + MA system enhances particle formation. In these reactions, although the concentration of gas-phase NH_3 was about 4 times higher than that of MA, the concentration of MA was about 2 times higher in the particles. These studies expand our understanding of acid−base-initiated NPF and illustrate the importance of combining experimental and theoretical approaches to better understand on a molecular level the mechanism of particle formation and growth in the atmosphere.

■ ASSOCIATED CONTENT

Supporting Information

The Supporting Information is available free of charge at https://pubs.acs.org/doi/10.1021/acsearthspacechem.0c00120.

Additional details on the experimental methods; stability of the size distribution of particles measured in the flow reactor over time; size distributions for the MSA + MA and MSA + MA + NH_3 nucleation systems as a function of residence time; comparison of size distributions measured for the MSA + NH_3, MSA + MA, and MSA + MA + NH_3 systems collected at ∼9 s; TDCIMS raw mass spectra obtained in the positive ion mode and negative ion mode; total integrated ion signal intensities for MA, NH_3, and MSA as a function of collection time; independent analysis of the MSA−MA-atomized particles; size-independent signal ratio between MSA and MA, and between MSA and NH_3, measured by TDCIMS for the atomized particles; and details on the determination of acid/base molar ratios from TDCIMS signal intensities (PDF).

■ AUTHOR INFORMATION

Corresponding Authors

James N. Smith − *Department of Chemistry, University of California, Irvine, Irvine, California 92697, United States;* orcid.org/0000-0003-4677-8224; Phone: (949) 824-9518; Email: jimsmith@uci.edu; Fax: (949) 824-2420

Barbara J. Finlayson-Pitts − *Department of Chemistry, University of California, Irvine, Irvine, California 92697, United States;* orcid.org/0000-0003-4650-168X; Phone: (949) 824-7670; Email: bjfinlay@uci.edu; Fax: (949) 824-2420

https://dx.doi.org/10.1021/acsearthspacechem.0c00120
ACS Earth Space Chem. 2020, 4, 1182−1194

Authors

Véronique Perraud − *Department of Chemistry, University of California, Irvine, Irvine, California 92697, United States;* orcid.org/0000-0003-1247-9787

Xiaoxiao Li − *Department of Chemistry, University of California, Irvine, Irvine, California 92697, United States; State Key Joint Laboratory of Environment Simulation and Pollution Control, School of Environment, Tsinghua University, Beijing 100084, China*

Jingkun Jiang − *State Key Joint Laboratory of Environment Simulation and Pollution Control, School of Environment, Tsinghua University, Beijing 100084, China;* orcid.org/0000-0001-6172-190X

Complete contact information is available at: https://pubs.acs.org/10.1021/acsearthspacechem.0c00120

Author Contributions

§V. P. and X. L. are equal first author contributors.

Notes

The authors declare no competing financial interest.

Data availability. Data for Figures 2, 4, and 5 are publicly available and archived at https://doi.org/10.7280/D1738J (Perraud et al., 2020).[127]

■ ACKNOWLEDGMENTS

The authors are grateful to the National Science Foundation (grant nos. 1928252 and CHE-1710580) for supporting this research. X.L. acknowledges funding from the China Scholarship Council. The authors would like to thank Prof. R. B. Gerber and Dr. J. Xu for helpful discussions on the theoretical calculations and M. Lawler for assistance with the data analysis using TTAP.

■ REFERENCES

(1) Kulmala, M.; Vehkamäki, H.; Petäjä, T.; Dal Maso, M.; Lauri, A.; Kerminen, V.-M.; Birmili, W.; McMurry, P. H. Formation and growth rates of ultrafine atmospheric particles: a review of observations. *J. Aerosol Sci.* **2004**, *35*, 143−176.

(2) Zhang, R.; Khalizov, A.; Wang, L.; Hu, M.; Xu, W. Nucleation and growth of nanoparticles in the atmosphere. *Chem. Rev.* **2012**, *112*, 1957−2011.

(3) Lee, S.-H.; Gordon, H.; Yu, H.; Lehtipalo, K.; Haley, R.; Li, Y.; Zhang, R. New particle formation in the atmosphere: from molecular clusters to global climate. *J. Geophys. Res.* **2019**, *124*, 7098−7146.

(4) Makkonen, R.; Asmi, A.; Kerminen, V.-M.; Boy, M.; Arneth, A.; Hari, P.; Kulmala, M. Air pollution control and decreasing new particle formation lead to strong climate warming. *Atmos. Chem. Phys.* **2012**, *12*, 1515−1524.

(5) Merikanto, J.; Spracklen, D. V.; Mann, G. W.; Pickering, S. J.; Carslaw, K. S. Impact of nucleation on global CCN. *Atmos. Chem. Phys.* **2009**, *9*, 8601−8616.

(6) Dunne, E. M.; Gordon, H.; Kürten, A.; Almeida, J.; Duplissy, J.; Williamson, C.; Ortega, I. K.; Pringle, K. J.; Adamov, A.; Baltensperger, U.; Barmet, P.; Benduhn, F.; Bianchi, F.; Breitenlechner, M.; Clarke, A.; Curtius, J.; Dommen, J.; Donahue, N. M.; Ehrhart, S.; Flagan, R. C.; Franchin, A.; Guida, R.; Hakala, J.; Hansel, A.; Heinritzi, M.; Jokinen, T.; Kangasluoma, J.; Kirkby, J.; Kulmala, M.; Kupc, A.; Lawler, M. J.; Lehtipalo, K.; Makhmutov, V.; Mann, G.; Mathot, S.; Merikanto, J.; Miettinen, P.; Nenes, A.; Onnela, A.; Rap, A.; Reddington, C. L. S.; Riccobono, F.; Richards, N. A. D.; Rissanen, M. P.; Rondo, L.; Sarnela, N.; Schobesberger, S.; Sengupta, K.; Simon, M.; Sipila, M.; Smith, J. N.; Stozkhov, Y.; Tome, A.; Trostl, J.; Wagner, P. E.; Wimmer, D.; Winkler, P. M.; Worsnop, D. R.; Carslaw, K. S. Global atmospheric particle formation from CERN CLOUD measurements. *Science* **2016**, *354*, 1119−1124.

(7) Yu, F.; Wang, Z.; Luo, G.; Turco, R. Ion-mediated nucleation as an important global source of tropospheric aerosols. *Atmos. Chem. Phys.* **2008**, *8*, 2537−2554.

(8) Kulmala, M.; Riipinen, I.; Sipila, M.; Manninen, H. E.; Petaja, T.; Junninen, H.; Maso, M. D.; Mordas, G.; Mirme, A.; Vana, M.; Hirsikko, A.; Laakso, L.; Harrison, R. M.; Hanson, I.; Leung, C.; Lehtinen, K. E. J.; Kerminen, V.-M. Toward direct measurement of atmospheric nucleation. *Science* **2007**, *318*, 89−92.

(9) Sipila, M.; Berndt, T.; Petaja, T.; Brus, D.; Vanhanen, J.; Stratmann, F.; Patokoski, J.; Mauldin, R. L.; Hyvarinen, A.-P.; Lihavainen, H.; Kulmala, M. The role of sulfuric acid in atmospheric nucleation. *Science* **2010**, *327*, 1243−1246.

(10) Zhang, R. Getting to the critical nucleus of aerosol formation. *Science* **2010**, *328*, 1366−1367.

(11) Kulmala, M.; Petäjä, T.; Ehn, M.; Thornton, J.; Sipilä, M.; Worsnop, D. R.; Kerminen, V.-M. Chemistry of atmospheric nucleation: on the recent advances on precursor characterization and atmospheric cluster composition in connection with atmospheric new particle formation. *Annu. Rev. Phys. Chem.* **2014**, *65*, 21−37.

(12) Curtius, J. Nucleation of atmospheric particles. *Eur. Phys. J. Conf.* **2009**, *1*, 199−209.

(13) Bowles, R. K.; McGraw, R.; Schaaf, P.; Senger, B.; Voegel, J.-C.; Reiss, H. A molecular based derivation of the nucleation theorem. *J. Chem. Phys.* **2000**, *113*, 4524−4532.

(14) McGraw, R.; Wu, D. T. Kinetic extensions of the nucleation theorem. *J. Chem. Phys.* **2003**, *118*, 9337−9347.

(15) Kerminen, V.-M.; Lihavainen, H.; Komppula, M.; Viisanen, Y.; Kulmala, M., Direct observational evidence linking atmospheric aerosol formation and cloud droplet activation. *Geophys. Res. Lett.* **2005**, *32* DOI: 10.1029/2005gl023130

(16) Dusek, U.; Frank, G. P.; Hildebrandt, L.; Curtius, J.; Schneider, J.; Walter, S.; Chand, D.; Drewnick, F.; Hings, S.; Jung, D.; Borrmann, S.; Andreae, M. O. Size matters more than chemistry for cloud-nucleating ability of aerosol particles. *Science* **2006**, *312*, 1375−1378.

(17) Pierce, J. R.; Adams, P. J. Efficiency of cloud condensation nuclei formation from ultrafine particles. *Atmos. Chem. Phys.* **2007**, *7*, 1367−1379.

(18) Singh, A.; Bloss, W. J.; Pope, F. D. 60 years of UK visibility measurements: impact of meteorology and atmospheric pollutants on visibility. *Atmos. Chem. Phys.* **2017**, *17*, 2085−2101.

(19) Chang, D.; Song, Y.; Liu, B. Visibility trends in six megacities in China 1973-2007. *Atmos. Res.* **2009**, *94*, 161−167.

(20) Hinds, W. C. *Aerosol Technology: Properties, Behavior and, Measurement of Airborne Particles*; John Wiley & Sons Inc.: New York, 1999.

(21) Pope, C. A.; Dockery, D. W. Health effects of fine particulate air pollution: Lines that connect. *J. Air Waste Manage. Assoc.* **2006**, *56*, 709−742.

(22) Pöschl, U. Atmospheric aerosols: Composition, transformation, climate and health effects. *Angew. Chem., Int. Ed.* **2005**, *44*, 7520−7540.

(23) Heal, M. R.; Kumar, P.; Harrison, R. M. Particles, air quality, policy and health. *Chem. Soc. Rev.* **2012**, *41*, 6606−6630.

(24) McMurry, P. H.; Friedlander, S. K. New particle formation in the presence of an aerosol. *Atmos. Environ.* **1979**, *13*, 1635−1651.

(25) Vehkamäki, H.; Riipinen, I. Thermodynamics and kinetics of atmospheric aerosol particle formation and growth. *Chem. Soc. Rev.* **2012**, *41*, 5160−5173.

(26) Bianchi, F.; Praplan, A. P.; Sarnela, N.; Dommen, J.; Kürten, A.; Ortega, I. K.; Schobesberger, S.; Junninen, H.; Simon, M.; Tröstl, J.; Jokinen, T.; Sipilä, M.; Adamov, A.; Amorim, A.; Almeida, J.; Breitenlechner, M.; Duplissy, J.; Ehrhart, S.; Flagan, R. C.; Franchin, A.; Hakala, J.; Hansel, A.; Heinritzi, M.; Kangasluoma, J.; Keskinen, H.; Kim, J.; Kirkby, J.; Laaksonen, A.; Lawler, M. J.; Lehtipalo, K.; Leiminger, M.; Makhmutov, V.; Mathot, S.; Onnela, A.; Petäjä, T.; Riccobono, F.; Rissanen, M. P.; Rondo, L.; Tomé, A.; Virtanen, A.; Viisanen, Y.; Williamson, C.; Wimmer, D.; Winkler, P. M.; Ye, P.; Curtius, J.; Kulmala, M.; Worsnop, D. R.; Donahue, N. M.; Baltensperger, U. Insight into acid-base nucleation experiments by

comparison of the chemical composition of positive, negative, and neutral clusters. *Environ. Sci. Technol.* **2014**, *48*, 13675−13684.
(27) Lehtipalo, K.; Rondo, L.; Kontkanen, J.; Schobesberger, S.; Jokinen, T.; Sarnela, N.; Kürten, A.; Ehrhart, S.; Franchin, A.; Nieminen, T.; Riccobono, F.; Sipilä, M.; Yli-Juuti, T.; Duplissy, J.; Adamov, A.; Ahlm, L.; Almeida, J.; Amorim, A.; Bianchi, F.; Breitenlechner, M.; Dommen, J.; Downard, A. J.; Dunne, E. M.; Flagan, R. C.; Guida, R.; Hakala, J.; Hansel, A.; Jud, W.; Kangasluoma, J.; Kerminen, V.-M.; Keskinen, H.; Kim, J.; Kirkby, J.; Kupc, A.; Kupiainen-Määttä, O.; Laaksonen, A.; Lawler, M. J.; Leiminger, M.; Mathot, S.; Olenius, T.; Ortega, I. K.; Onnela, A.; Petäjä, T.; Praplan, A.; Rissanen, M. P.; Ruuskanen, T.; Santos, F. D.; Schallhart, S.; Schnitzhofer, R.; Simon, M.; Smith, J. N.; Tröstl, J.; Tsagkogeorgas, G.; Tomé, A.; Vaattovaara, P.; Vehkamäki, H.; Vrtala, A. E.; Wagner, P. E.; Williamson, C.; Wimmer, D.; Winkler, P. M.; Virtanen, A.; Donahue, N. M.; Carslaw, K. S.; Baltensperger, U.; Riipinen, I.; Curtius, J.; Worsnop, D. R.; Kulmala, M. The effect of acid-base clustering and ions on the growth of atmospheric nano-particles. *Nat. Commun.* **2016**, *7*, 1−9.
(28) Chen, M.; Titcombe, M.; Jiang, J.; Jen, C.; Kuang, C.; Fischer, M. L.; Eisele, F. L.; Siepmann, J. I.; Hanson, D. R.; Zhao, J. Acid−base chemical reaction model for nucleation rates in the polluted atmospheric boundary layer. *Proc. Natl. Acad. Sci. U.S.A.* **2012**, *109*, 18713−18718.
(29) Kim, T. O.; Ishida, T.; Adachi, M.; Okuyama, K.; Seinfeld, J. H. Nanometer-sized particle formation from $NH_3/SO_2/H_2O$/Air mixtures by ionizing irradiation. *Aerosol Sci. Technol.* **1998**, *29*, 111−125.
(30) Korhonen, P.; Kulmala, M.; Laaksonen, A.; Viisanen, Y.; McGraw, R.; Seinfeld, J. H. Ternary nucleation of H_2SO_4, NH_3, and H_2O in the atmosphere. *J. Geophys. Res.* **1999**, *104*, 26349−26353.
(31) Chen, H.; Varner, M. E.; Gerber, R. B.; Finlayson-Pitts, B. J. Reactions of methanesulfonic acid with amines and ammonia as a source of new particles in air. *J. Phys. Chem. B* **2016**, *120*, 1526−1536.
(32) Chen, H.; Finlayson-Pitts, B. J. New particle formation from methanesulfonic acid and amines/ammonia as a function of temperature. *Environ. Sci. Technol.* **2017**, *51*, 243−252.
(33) Dawson, M. L.; Varner, M. E.; Perraud, V.; Ezell, M. J.; Gerber, R. B.; Finlayson-Pitts, B. J. Simplified mechanism for new particle formation from methanesulfonic acid, amines, and water via experiments and ab initio calculations. *Proc. Natl. Acad. Sci. U.S.A.* **2012**, *109*, 18719−18724.
(34) Almeida, J.; Schobesberger, S.; Kürten, A.; Ortega, I. K.; Kupiainen-Määttä, O.; Praplan, A. P.; Adamov, A.; Amorim, A.; Bianchi, F.; Breitenlechner, M.; David, A.; Dommen, J.; Donahue, N. M.; Downard, A.; Dunne, E.; Duplissy, J.; Ehrhart, S.; Flagan, R. C.; Franchin, A.; Guida, R.; Hakala, J.; Hansel, A.; Heinritzi, M.; Henschel, H.; Jokinen, T.; Junninen, H.; Kajos, M.; Kangasluoma, J.; Keskinen, H.; Kupc, A.; Kurtén, T.; Kvashin, A. N.; Laaksonen, A.; Lehtipalo, K.; Leiminger, M.; Leppä, J.; Loukonen, V.; Makhmutov, V.; Mathot, S.; McGrath, M. J.; Nieminen, T.; Olenius, T.; Onnela, A.; Petäjä, T.; Riccobono, F.; Riipinen, I.; Rissanen, M.; Rondo, L.; Ruuskanen, T.; Santos, F. D.; Sarnela, N.; Schallhart, S.; Schnitzhofer, R.; Seinfeld, J. H.; Simon, M.; Sipilä, M.; Stozhkov, Y.; Stratmann, F.; Tomé, A.; Tröstl, J.; Tsagkogeorgas, G.; Vaattovaara, P.; Viisanen, Y.; Virtanen, A.; Vrtala, A.; Wagner, P. E.; Weingartner, E.; Wex, H.; Williamson, C.; Wimmer, D.; Ye, P.; Yli-Juuti, T.; Carslaw, K. S.; Kulmala, M.; Curtius, J.; Baltensperger, U.; Worsnop, D. R.; Vehkamäki, H.; Kirkby, J. Molecular understanding of sulphuric acid-amine particle nucleation in the atmosphere. *Nature* **2013**, *502*, 359−363.
(35) Arquero, K. D.; Gerber, R. B.; Finlayson-Pitts, B. J. The role of oxalic acid in new particle formation from methanesulfonic acid, methylamine, and water. *Environ. Sci. Technol.* **2017**, *51*, 2124−2130.
(36) Arquero, K. D.; Xu, J.; Gerber, R. B.; Finlayson-Pitts, B. J. Particle formation and growth from oxalic acid, methanesulfonic acid, trimethylamine and water: a combined experimental and theoretical study. *Phys. Chem. Chem. Phys.* **2017**, *19*, 28286−28301.
(37) Chen, H.; Ezell, M. J.; Arquero, K. D.; Varner, M. E.; Dawson, M. L.; Gerber, R. B.; Finlayson-Pitts, B. J. New particle formation and growth from methanesulfonic acid, trimethylamine and water. *Phys. Chem. Chem. Phys.* **2015**, *17*, 13699−13709.
(38) Kumar, M.; Francisco, J. S. Ion pair particles at the air-water interface. *Proc. Natl. Acad. Sci. U.S.A.* **2017**, *114*, 12401−12406.
(39) Kettle, A. J.; Rhee, T. S.; von Hobe, M.; Poulton, A.; Aiken, J.; Andreae, M. O. Assessing the flux of different volatile sulfur gases from the ocean to the atmosphere. *J. Geophys. Res.* **2001**, *106*, 12193−12209.
(40) Trabue, S.; Scoggin, K.; Mitloehner, F.; Li, H.; Burns, R.; Xin, H. Field sampling method for quantifying volatile sulfur compounds from animal feeding operations. *Atmos. Environ.* **2008**, *42*, 3332−3341.
(41) Lamb, B.; Westberg, H.; Allwine, G.; Bamesberger, L.; Guenther, A. Measurement of biogenic sulfur emissions from soils and vegetation - Application of dynamic enclosure methods with Natusch filter and GC/FPD analysis. *J. Atmos. Chem.* **1987**, *5*, 469−491.
(42) Bates, T. S.; Lamb, B. K.; Guenther, A.; Dignon, J.; Stoiber, R. E. Sulfur emissions to the atmosphere from natural sources. *J. Atmos. Chem.* **1992**, *14*, 315−337.
(43) Perraud, V.; Meinardi, S.; Blake, D. R.; Finlayson-Pitts, B. J. Challenges associated with the sampling and analysis of organosulfur compounds in air using real-time PTR-ToF-MS and offline GC-FID. *Atmos. Meas. Tech.* **2016**, *9*, 1325−1340.
(44) De Bruyn, W. J.; Bates, T. S.; Cainey, J. M.; Saltzman, E. S. Shipboard measurements of dimethyl sulfide and SO_2 southwest of Tasmania during the First Aerosol Characterization Experiment (ACE 1). *J. Geophys. Res.* **1998**, *103*, 16703−16711.
(45) Marandino, C. A.; De Bruyn, W. J.; Miller, S. D.; Saltzman, E. S. Open ocean DMS air/sea fluxes over the eastern South Pacific Ocean. *Atmos. Chem. Phys.* **2009**, *9*, 345−356.
(46) Berresheim, H.; Elste, T.; Tremmel, H. G.; Allen, A. G.; Hansson, H. C.; Rosman, K.; Dal Maso, M.; Makela, J. M.; Kulmala, M.; O'Dowd, C. D. Gas-aerosol relationships of H_2SO_4, MSA, and OH: Observations in the coastal marine boundary layer at Mace Head, Ireland. *J. Geophys. Res.* **2002**, *107*, PAR 5-1−PAR 5-12.
(47) Eisele, F. L.; Tanner, D. J. Measurement of the gas-phase concentration of H_2SO_4 and methane sulfonic acid and estimates of H_2SO_4 production and loss in the atmosphere. *J. Geophys. Res.* **1993**, *98*, 9001−9010.
(48) Jefferson, A.; Tanner, D. J.; Eisele, F. L.; Davis, D. D.; Chen, G.; Crawford, J.; Huey, J. W.; Torres, A. L.; Berresheim, H. OH photochemistry and methane sulfonic acid formation in the coastal Antarctic boundary layer. *J. Geophys. Res.* **1998**, *103*, 1647−1656.
(49) Berresheim, H.; Adam, M.; Monahan, C.; O'Dowd, C.; Plane, J. M. C.; Bohn, B.; Rohrer, F. Missing SO_2 oxidant in the coastal atmosphere? - Observations from high-resolution measurements of OH and atmospheric sulfur compounds. *Atmos. Chem. Phys.* **2014**, *14*, 12209−12223.
(50) Lawler, M. J.; Rissanen, M. P.; Ehn, M.; Mauldin, R. L.; Sarnela, N.; Sipilä, M.; Smith, J. N. Evidence for diverse biogeochemical drivers of boreal forest new particle formation. *Geophys. Res. Lett.* **2018**, *45*, 2038−2046.
(51) Kerminen, V.-M.; Aurela, M.; Hillamo, R. E.; Virkkula, A. Formation of particulate MSA: Deductions from size distribution measurements in the Finnish Arctic. *Tellus B* **1997**, *49*, 159−171.
(52) Dall'Osto, M.; Beddows, D. C. S.; Tunved, P.; Krejci, R.; Strom, J.; Hansson, H. C.; Yoon, Y. J.; Park, K. T.; Becagli, S.; Udisti, R.; Onasch, T.; O'Dowd, C. D.; Simo, R.; Harrison, R. M. Arctic sea ice melt leads to atmospheric new particle formation. *Sci. Rep.* **2017**, *7*, 1−10.
(53) Quinn, P. K.; Miller, T. L.; Bates, T. S.; Ogren, J. A.; Andrews, E.; Shaw, G. E. A 3-year record of simultaneously measured aerosol chemical and optical properties at Barrow, Alaska. *J. Geophys. Res.* **2002**, *107*, AAC 8-1−AAC 8-15.
(54) Leaitch, W. R.; Sharma, S.; Huang, L.; Toom-Sauntry, D.; Chivulescu, A.; Macdonald, A.-M.; von Salzen, K.; Pierce, J. R.;

Bertram, A. K.; Schroder, J. C.; Shantz, N. C.; Chang, R. Y.-W.; Norman, A.-L. Dimethyl sulfide control of the clean summertime Arctic aerosol and cloud. *Elementa Sci. Anthrop.* **2013**, *1*, 000017.
(55) Perraud, V.; Horne, J. R.; Martinez, A. S.; Kalinowski, J.; Meinardi, S.; Dawson, M. L.; Wingen, L. M.; Dabdub, D.; Blake, D. R.; Gerber, R. B.; Finlayson-Pitts, B. J. The future of airborne sulfur-containing particles in the absence of fossil fuel sulfur dioxide emissions. *Proc. Natl. Acad. Sci. U.S.A.* **2015**, *112*, 13514−13519.
(56) Klimont, Z.; Smith, S. J.; Cofala, J. The last decade of global anthropogenic sulfur dioxide: 2000-2011 emissions. *Environ. Res. Lett.* **2013**, *8*, 014003.
(57) Murphy, J. G.; Gregoire, P. K.; Tevlin, A. G.; Wentworth, G. R.; Ellis, R. A.; Markovic, M. Z.; VandenBoer, T. C. Observational constraints on particle acidity using measurements and modelling of particles and gases. *Faraday Discuss.* **2017**, *200*, 379−395.
(58) U.S. EPA. https://www.epa.gov/air-trends/sulfur-dioxide-trends (accessed Sept. 16, 2019).
(59) Amann, M.; Klimont, Z.; Wagner, F. Regional and global emissions of air pollutants: Recent trends and future scenarios. *Annu. Rev. Environ. Resour.* **2013**, *38*, 31−55.
(60) Stern, D. I. Global sulfur emissions from 1850 to 2000. *Chemosphere* **2005**, *58*, 163−175.
(61) Sharma, S.; Chan, E.; Ishizawa, M.; Toom-Sauntry, D.; Gong, S. L.; Li, S. M.; Tarasick, D. W.; Leaitch, W. R.; Norman, A.; Quinn, P. K.; Bates, T. S.; Levasseur, M.; Barrie, L. A.; Maenhaut, W., Influence of transport and ocean ice extent on biogenic aerosol sulfur in the Arctic atmosphere. *J. Geophys. Res.* **2012**, *117*, No. a (1-12). DOI: 10.1029/2011jd017074
(62) Becagli, S.; Lazzara, L.; Marchese, C.; Dayan, U.; Ascanius, S. E.; Cacciani, M.; Caiazzo, L.; Di Biagio, C.; Di Iorio, T.; di Sarra, A.; Eriksen, P.; Fani, F.; Giardi, F.; Meloni, D.; Muscari, G.; Pace, G.; Severi, M.; Traversi, R.; Udisti, R. Relationships linking primary production, sea ice melting, and biogenic aerosol in the Arctic. *Atmos. Environ.* **2016**, *136*, 1−15.
(63) Abbatt, J. P. D.; Leaitch, W. R.; Aliabadi, A. A.; Bertram, A. K.; Blanchet, J.-P.; Boivin-Rioux, A.; Bozem, H.; Burkart, J.; Chang, R. Y. W.; Charette, J.; Chaubey, J. P.; Christensen, R. J.; Cirisan, A.; Collins, D. B.; Croft, B.; Dionne, J.; Evans, G. J.; Fletcher, C. G.; Galí, M.; Ghahremaninezhad, R.; Girard, E.; Gong, W.; Gosselin, M.; Gourdal, M.; Hanna, S. J.; Hayashida, H.; Herber, A. B.; Hesaraki, S.; Hoor, P.; Huang, L.; Hussherr, R.; Irish, V. E.; Keita, S. A.; Kodros, J. K.; Köllner, F.; Kolonjari, F.; Kunkel, D.; Ladino, L. A.; Law, K.; Levasseur, M.; Libois, Q.; Liggio, J.; Lizotte, M.; Macdonald, K. M.; Mahmood, R.; Martin, R. V.; Mason, R. H.; Miller, L. A.; Moravek, A.; Mortenson, E.; Mungall, E. L.; Murphy, J. G.; Namazi, M.; Norman, A.-L.; O'Neill, N. T.; Pierce, J. R.; Russell, L. M.; Schneider, J.; Schulz, H.; Sharma, S.; Si, M.; Staebler, R. M.; Steiner, N. S.; Thomas, J. L.; von Salzen, K.; Wentzell, J. J. B.; Willis, M. D.; Wentworth, G. R.; Xu, J.-W.; Yakobi-Hancock, J. D. Overview paper: New insights into aerosol and climate in the Arctic. *Atmos. Chem. Phys.* **2019**, *19*, 2527−2560.
(64) Rempillo, O.; Seguin, A. M.; Norman, A. L.; Scarratt, M.; Michaud, S.; Chang, R.; Sjostedt, S.; Abbatt, J.; Else, B.; Papakyriakou, T.; Sharma, S.; Grasby, S.; Levasseur, M., Dimethyl sulfide air-sea fluxes and biogenic sulfur as a source of new aerosols in the Arctic fall. *J. Geophys. Res.* **2011**, *116*. DOI: 10.1029/2011jd016336
(65) Ge, X.; Wexler, A. S.; Clegg, S. L. Atmospheric amines - Part I. A review. *Atmos. Environ.* **2011**, *45*, 524−546.
(66) Dawson, M. L.; Perraud, V.; Gomez, A.; Arquero, K. D.; Ezell, M. J.; Finlayson-Pitts, B. J. Measurement of gas-phase ammonia and amines in air by collection onto an ion exchange resin and analysis by ion chromatography. *Atmos. Meas. Tech.* **2014**, *7*, 2733−2744.
(67) Schade, G. W.; Crutzen, P. J. Emission of aliphatic-amines from animal husbandry and their reactions - potential source of N_2O and HCN. *J. Atmos. Chem.* **1995**, *22*, 319−346.
(68) Van Neste, A.; Duce, R. A.; Lee, C. Methylamines in the marine atmosphere. *Geophys. Res. Lett.* **1987**, *14*, 711−714.
(69) Yu, H.; Lee, S.-H. Chemical ionisation mass spectrometry for the measurement of atmospheric amines. *Environ. Chem.* **2012**, *9*, 190−201.
(70) Hellén, H.; Kieloaho, A.-J.; Hakola, H. Gas-phase alkyl amines in urban air; comparison with a boreal forest site and importance for local atmospheric chemistry. *Atmos. Environ.* **2014**, *94*, 192−197.
(71) Hanson, D. R.; McMurry, P. H.; Jiang, J.; Tanner, D.; Huey, L. G. Ambient pressure proton transfer mass spectrometry: detection of amines and ammonia. *Environ. Sci. Technol.* **2011**, *45*, 8881−8888.
(72) VandenBoer, T. C.; Petroff, A.; Markovic, M. Z.; Murphy, J. G. Size distribution of alkyl amines in continental particulate matter and their online detection in the gas and particle phase. *Atmos. Chem. Phys.* **2011**, *11*, 4319−4332.
(73) You, Y.; Kanawade, V. P.; de Gouw, J. A.; Guenther, A. B.; Madronich, S.; Sierra-Hernández, M. R.; Lawler, M.; Smith, J. N.; Takahama, S.; Ruggeri, G.; Koss, A.; Olson, K.; Baumann, K.; Weber, R. J.; Nenes, A.; Guo, H.; Edgerton, E. S.; Porcelli, L.; Brune, W. H.; Goldstein, A. H.; Lee, S.-H. Atmospheric amines and ammonia measured with a chemical ionization mass spectrometer (CIMS). *Atmos. Chem. Phys.* **2014**, *14*, 12181−12194.
(74) Croft, B.; Wentworth, G. R.; Martin, R. V.; Leaitch, W. R.; Murphy, J. G.; Murphy, B. N.; Kodros, J. K.; Abbatt, J. P. D.; Pierce, J. R. Contribution of Arctic seabird-colony ammonia to atmospheric particles and cloud-albedo radiative effect. *Nat. Commun.* **2016**, *7*, 1−10.
(75) Wentworth, G. R.; Murphy, J. G.; Croft, B.; Martin, R. V.; Pierce, J. R.; Côté, J.-S.; Courchesne, I.; Tremblay, J.-É.; Gagnon, J.; Thomas, J. L.; Sharma, S.; Toom-Sauntry, D.; Chivulescu, A.; Levasseur, M.; Abbatt, J. P. D. Ammonia in the summertime Arctic marine boundary layer: sources, sinks, and implications. *Atmos. Chem. Phys.* **2016**, *16*, 1937−1953.
(76) Kurtén, T.; Loukonen, V.; Vehkamäki, H.; Kulmala, M. Amines are likely to enhance neutral and ion-induced sulfuric acid-water nucleation in the atmosphere more effectively than ammonia. *Atmos. Chem. Phys.* **2008**, *8*, 4095−4103.
(77) Yu, H.; McGraw, R.; Lee, S.-H., Effects of amines on formation of sub-3 nm particles and their subsequent growth. *Geophys. Res. Lett.* **2012**, *39*, No. L02807 (1-5). DOI: 10.1029/2011gl050099
(78) Glasoe, W. A.; Volz, K.; Panta, B.; Freshour, N.; Bachman, R.; Hanson, D. R.; McMurry, P. H.; Jen, C. Sulfuric acid nucleation: An experimental study of the effect of seven bases. *J. Geophys. Res.* **2015**, *120*, 1933−1950.
(79) Zollner, J. H.; Glasoe, W. A.; Panta, B.; Carlson, K. K.; McMurry, P. H.; Hanson, D. R. Sulfuric acid nucleation: power dependencies, variation with relative humidity, and effect of bases. *Atmos. Chem. Phys.* **2012**, *12*, 4399−4411.
(80) Jen, C. N.; McMurry, P. H.; Hanson, D. R. Stabilization of sulfuric acid dimers by ammonia, methylamine, dimethylamine, and trimethylamine. *J. Geophys. Res.* **2014**, *119*, 7502−7514.
(81) Bzdek, B. R.; Ridge, D. P.; Johnston, M. V. Amine exchange into ammonium bisulfate and ammonium nitrate nuclei. *Atmos. Chem. Phys.* **2010**, *10*, 3495−3503.
(82) Liu, Y.; Han, C.; Liu, C.; Ma, J.; Ma, Q.; He, H. Differences in the reactivity of ammonium salts with methylamine. *Atmos. Chem. Phys.* **2012**, *12*, 4855−4865.
(83) Qiu, C.; Wang, L.; Lal, V.; Khalizov, A. F.; Zhang, R. Heterogeneous reactions of alkylamines with ammonium sulfate and ammonium bisulfate. *Environ. Sci. Technol.* **2011**, *45*, 4748−4755.
(84) Bzdek, B. R.; Ridge, D. P.; Johnston, M. V., Reactivity of methanesulfonic acid salt clusters relevant to marine air. *J. Geophys. Res.* **2011**, *116*, No. D03301 (1-7). DOI: 10.1029/2010jd015217
(85) Myllys, N.; Chee, S.; Olenius, T.; Lawler, M.; Smith, J. Molecular-level understanding of synergistic effects in sulfuric acid-amine-ammonia mixed clusters. *J. Phys. Chem. A* **2019**, *123*, 2420−2425.
(86) Temelso, B.; Morrison, E. F.; Speer, D. L.; Cao, B. C.; Appiah-Padi, N.; Kim, G.; Shields, G. C. Effect of mixing ammonia and alkylamines on sulfate aerosol formation. *J. Phys. Chem. A* **2018**, *122*, 1612−1622.

(87) Perraud, V.; Xu, J.; Gerber, R. B.; Finlayson-Pitts, B. J. Integrated experimental and theoretical approach to probe the synergistic effect of ammonia in methanesulfonic acid reactions with small alkylamines. *Environ. Sci. Processes Impacts* **2020**, *22*, 305−328.
(88) Chen, D.; Wang, W.; Li, D.; Wang, W. Atmospheric implication of synergy in methanesulfonic acid-base trimers: a theoretical investigation. *RSC Adv.* **2020**, *10*, 5173−5182.
(89) Köllner, F.; Schneider, J.; Willis, M. D.; Klimach, T.; Helleis, F.; Bozem, H.; Kunkel, D.; Hoor, P.; Burkart, J.; Leaitch, W. R.; Aliabadi, A. A.; Abbatt, J. P. D.; Herber, A. B.; Borrmann, S. Particulate trimethylamine in the summertime Canadian high Arctic lower troposphere. *Atmos. Chem. Phys.* **2017**, *17*, 13747−13766.
(90) Facchini, M. C.; Decesari, S.; Rinaldi, M.; Carbone, C.; Finessi, E.; Mircea, M.; Fuzzi, S.; Moretti, F.; Tagliavini, E.; Ceburnis, D.; O'Dowd, C. D. Important source of marine secondary organic aerosol from biogenic amines. *Environ. Sci. Technol.* **2008**, *42*, 9116−9121.
(91) Gaston, C. J.; Pratt, K. A.; Qin, X.; Prather, K. A. Real-time detection and mixing state of methanesulfonate in single particles at an inland urban location during a phytoplankton bloom. *Environ. Sci. Technol.* **2010**, *44*, 1566−1572.
(92) Müller, C.; Iinuma, Y.; Karstensen, J.; van Pinxteren, D.; Lehmann, S.; Gnauk, T.; Herrmann, H. Seasonal variation of aliphatic amines in marine sub-micrometer particles at the Cape Verde islands. *Atmos. Chem. Phys.* **2009**, *9*, 9587−9597.
(93) Sorooshian, A.; Padro, L. T.; Nenes, A.; Feingold, G.; McComiskey, A.; Hersey, S. P.; Gates, H.; Jonsson, H. H.; Miller, S. D.; Stephens, G. L.; Flagan, R. C.; Seinfeld, J. H. On the link between ocean biota emissions, aerosol, and maritime clouds: Airborne, ground, and satellite measurements off the coast of California. *Global Biogeochem. Cycles* **2009**, *23*, 1−15.
(94) Wang, S.; Johnston, M. V. Airborne nanoparticle characterization with a digital ion trap-reflectron time of flight mass spectrometer. *Int. J. Mass Spectrom.* **2006**, *258*, 50−57.
(95) Wang, S.; Zordan, C. A.; Johnston, M. V. Chemical characterization of individual, airborne sub-10-nm particles and molecules. *Anal. Chem.* **2006**, *78*, 1750−1754.
(96) Voisin, D.; Smith, J. N.; Sakurai, H.; McMurry, P. H.; Eisele, F. L. Thermal desorption chemical ionization mass spectrometer for ultrafine particle chemical composition. *Aerosol Sci. Technol.* **2003**, *37*, 471−475.
(97) Smith, J. N.; Barsanti, K. C.; Friedli, H. R.; Ehn, M.; Kulmala, M.; Collins, D. R.; Scheckman, J. H.; Williams, B. J.; McMurry, P. H. Observations of aminium salts in atmospheric nanoparticles and possible climatic implications. *Proc. Natl. Acad. Sci. U.S.A.* **2010**, *107*, 6634−6639.
(98) Smith, J. N.; Dunn, M. J.; VanReken, T. M.; Iida, K.; Stolzenburg, M. R.; McMurry, P. H.; Huey, L. G., Chemical composition of atmospheric nanoparticles formed from nucleation in Tecamac, Mexico: Evidence for an important role for organic species in nanoparticle growth. *Geophys. Res. Lett.* **2008**, *35*, No. L04808 (1-5). DOI: 10.1029/2007gl032523
(99) Smith, J. N.; Moore, K. F.; Eisele, F. L.; Voisin, D.; Ghimire, A. K.; Sakurai, H.; McMurry, P. H., Chemical composition of atmospheric nanoparticles during nucleation events in Atlanta. *J. Geophys. Res.* **2005**, *110*, No. D22S03 (1-13). DOI: 10.1029/2005jd005912
(100) Smith, J. N.; Moore, K. F.; McMurry, P. H.; Eisele, F. L. Atmospheric measurements of sub-20 nm diameter particle chemical composition by thermal desorption chemical ionization mass spectrometry. *Aerosol Sci. Technol.* **2004**, *38*, 100−110.
(101) Lawler, M. J.; Winkler, P. M.; Kim, J.; Ahlm, L.; Tröstl, J.; Praplan, A. P.; Schobesberger, S.; Kürten, A.; Kirkby, J.; Bianchi, F.; Duplissy, J.; Hansel, A.; Jokinen, T.; Keskinen, H.; Lehtipalo, K.; Leiminger, M.; Petäjä, T.; Rissanen, M.; Rondo, L.; Simon, M.; Sipilä, M.; Williamson, C.; Wimmer, D.; Riipinen, I.; Virtanen, A.; Smith, J. N. Unexpectedly acidic nanoparticles formed in dimethylamine-ammonia-sulfuric-acid nucleation experiments at CLOUD. *Atmos. Chem. Phys.* **2016**, *16*, 13601−13618.
(102) Chen, H.; Chee, S.; Lawler, M. J.; Barsanti, K. C.; Wong, B. M.; Smith, J. N. Size resolved chemical composition of nanoparticles from reactions of sulfuric acid with ammonia and dimethylamine. *Aerosol Sci. Technol.* **2018**, *52*, 1120−1133.
(103) Chee, S.; Myllys, N.; Barsanti, K. C.; Wong, B. M.; Smith, J. N. An experimental and modeling study of nanoparticle formation and growth from dimethylamine and nitric acid. *J. Phys. Chem. A* **2019**, *123*, 5640−5648.
(104) Kim, J.; Ahlm, L.; Yli-Juuti, T.; Lawler, M.; Keskinen, H.; Tröstl, J.; Schobesberger, S.; Duplissy, J.; Amorim, A.; Bianchi, F.; Donahue, N. M.; Flagan, R. C.; Hakala, J.; Heinritzi, M.; Jokinen, T.; Kürten, A.; Laaksonen, A.; Lehtipalo, K.; Miettinen, P.; Petäjä, T.; Rissanen, M. P.; Rondo, L.; Sengupta, K.; Simon, M.; Tomé, A.; Williamson, C.; Wimmer, D.; Winkler, P. M.; Ehrhart, S.; Ye, P.; Kirkby, J.; Curtius, J.; Baltensperger, U.; Kulmala, M.; Lehtinen, K. E. J.; Smith, J. N.; Riipinen, I.; Virtanen, A. Hygroscopicity of nanoparticles produced from homogeneous nucleation in the CLOUD experiments. *Atmos. Chem. Phys.* **2016**, *16*, 293−304.
(105) Chen, D.-R.; Pui, D. Y. A high efficiency, high throughput unipolar aerosol charger for nanoparticles. *J. Nanopart. Res.* **1999**, *1*, 115−126.
(106) McMurry, P. H.; Ghimire, A.; Ahn, H.-K.; Sakurai, H.; Moore, K.; Stolzenburg, M.; Smith, J. N. Sampling nanoparticles for chemical analysis by low resolution electrical mobility classification. *Environ. Sci. Technol.* **2009**, *43*, 4653−4658.
(107) Perraud, V.; Li, X.; Smith, J. N.; Finlayson-Pitts, B. J. Novel ionization reagent for the measurement of gas phase ammonia and amines using a standalone atmospheric pressure gas chromatography (APGC) source. *Rapid Commun. Mass Spectrom.* **2020**, *34*, 1−12.
(108) Fernandez, A. E.; Lewis, G. S.; Hering, S. V. Design and laboratory evaluation of a sequential spot sampler for time-resolved measurement of airborne particle composition. *Aerosol Sci. Technol.* **2014**, *48*, 655−663.
(109) Hecobian, A.; Evanoski-Cole, A.; Eiguren-Fernandez, A.; Sullivan, A. P.; Lewis, G. S.; Hering, S. V.; Collett, J. L., Jr. Evaluation of the Sequential Spot Sampler (S3) for time-resolved measurement of PM2.5 sulfate and nitrate through lab and field measurements. *Atmos. Meas. Tech.* **2016**, *9*, 525−533.
(110) Xu, J.; Perraud, V.; Finlayson-Pitts, B. J.; Gerber, R. B. Uptake of water by an acid-base nanoparticle: theoretical and experimental studies of the methanesulfonic acid-methylamine system. *Phys. Chem. Chem. Phys.* **2018**, *20*, 22249−22259.
(111) Kwong, K. C.; Chim, M. M.; Hoffmann, E. H.; Tilgner, A.; Herrmann, H.; Davies, J. F.; Wilson, K. R.; Chan, M. N. Chemical transformation of methanesulfonic acid and sodium methanesulfonate through heterogeneous OH oxidation. *ACS Earth Space Chem.* **2018**, *2*, 895−903.
(112) Rumble, J. R. *CRC Handbook of Chemistry and Physics*, (Internet Version 2019), 100th ed.; CRC Press/Taylor & Francis: Boca Raton, FL, 2019.
(113) Fehsenfeld, F. C.; Ferguson, E. E. Laboratory studies of negative-ion reactions with atmospheric trace constituents. *J. Chem. Phys.* **1974**, *61*, 3181−3193.
(114) Vacher, J. R.; Jorda, M.; Le Duc, E.; Fitaire, M. A determination of the stabilities of negative-ion clusters in SO_2 and SO_2-O_2 Mixtures. *Int. J. Mass Spectrom. Ion Processes* **1992**, *114*, 149−162.
(115) Stull, D. R. Vapor pressure of pure substances - Organic compounds. *Ind. Eng. Chem.* **1947**, *39*, 517−540.
(116) Tang, I. N.; Munkelwitz, H. R. Determination of vapor-pressure from droplet evaporation kinetics. *J. Colloid Interface Sci.* **1991**, *141*, 109−118.
(117) Tikkanen, O.-P.; Väisänen, O.; Hao, L.; Holopainen, E.; Wang, H.; Lehtinen, K. E. J.; Virtanen, A.; Yli-Juuti, T. Hygroscopicity of dimethylaminium-, sulfate-, and ammonium-containing nanoparticles. *Aerosol Sci. Technol.* **2018**, *52*, 971−983.
(118) Xu, J.; Finlayson-Pitts, B. J.; Gerber, R. B. Nanoparticles grown from methanesulfonic acid and methylamine: microscopic

structures and formation mechanism. *Phys. Chem. Chem. Phys.* **2017**, *19*, 31949−31957.
(119) Barsanti, K. C.; McMurry, P. H.; Smith, J. N. The potential contribution of organic salts to new particle growth. *Atmos. Chem. Phys.* **2009**, *9*, 2949−2957.
(120) Bzdek, B. R.; DePalma, J. W.; Johnston, M. V. Mechanisms of atmospherically relevant cluster growth. *Acc. Chem. Res.* **2017**, *50*, 1965−1975.
(121) DePalma, J. W.; Bzdek, B. R.; Ridge, D. P.; Johnston, M. V. Activation barriers in the growth of molecular clusters derived from sulfuric acid and ammonia. *J. Phys. Chem. A* **2014**, *118*, 11547−11554.
(122) Shen, J.; Xie, H.-B.; Elm, J.; Ma, F.; Chen, J.; Vehkamäki, H. Methanesulfonic acid-driven new particle formation enhanced by monoethanolamine: A computational study. *Environ. Sci. Technol.* **2019**, *53*, 14387−14397.
(123) Jen, C. N.; Zhao, J.; McMurry, P. H.; Hanson, D. R. Chemical ionization of clusters formed from sulfuric acid and dimethylamine or diamines. *Atmos. Chem. Phys.* **2016**, *16*, 12513−12529.
(124) Hunter, E. P. L.; Lias, S. G. Evaluated gas phase basicities and proton affinities of molecules: An update. *J. Phys. Chem. Ref. Data* **1998**, *27*, 413−656.
(125) Li, S.; Zhang, L.; Qin, W.; Tao, F.-M. Intermolecular structure and properties of the methanesulfonic acid-ammonia system in small water clusters. *Chem. Phys. Lett.* **2007**, *447*, 33−38.
(126) Olenius, T.; Kupiainen-Määttä, O.; Ortega, I. K.; Kurtén, T.; Vehkamäki, H. Free energy barrier in the growth of sulfuric acid-ammonia and sulfuric acid-dimethylamine clusters. *J. Chem. Phys.* **2013**, *139*, 084312.
(127) Perraud, V.; Li, X.; Jiang, J.; Smith, J. N.; Finlayson-Pitts, B. J. *Supplementary data for size-resolved chemical composition of sub-20 nm particles from methanesulfonic acid with methylamine and ammonia*, UC Irvine DRYAD, Dataset, DOI: 10.7280/D1738J.

https://dx.doi.org/10.1021/acsearthspacechem.0c00120
ACS Earth Space Chem. 2020, 4, 1182−1194